



Crashworthiness investigation on a Carbon Fiber Reinforced Plastic solar vehicle

Alessandro Papavassiliou, Ana Pavlovic^{*}, Giangiacomo Minak

Department of Industrial Engineering, University of Bologna, via Fontanelle 40, Forlì, Italy

ARTICLE INFO

Keywords:

Crash test
Ansys LS-Dyna
FEM simulation
CFRP
Solar vehicle

ABSTRACT

This article presents a research study involving different simulations of crash tests by means of the finite element explicit dynamic software Ansys LS-Dyna to determine the roadworthiness of a fully composite chassis lightweight solar vehicle and its conformity to the World Solar Challenge (WSC) regulations. Furthermore, the paper describes the results of crash test simulations in conditions comparable with those of the standard homologation test, with an initial velocity of 15.5 m/s against a rigid barrier considering overlaps of 50% and 100%. The velocity measured at the base of the seat was later used in a sled test with a dummy to calculate the Head Injury Criterion (HIC), a number proportional to the probability of head injury caused by the impact. The values remained within the threshold of acceptability with overlap at 50% but exceeded the limit with the 100% overlap. With no load limiter implemented in the model, the seatbelt caused contact forces with the chest up to 14 kN against 6 kN of the typical load limiter used in road cars to limit damage to ribs and internal organs. Finally, the possibility of improving the front crash box was investigated by changing the crash box's planar sandwich structure with corrugated ones and layup without foam between the carbon layers. Various values of semi-amplitudes (A) of the sinusoidal profile have been tested. With a value of A of 6 mm, the capacity to absorb energy from an impact at 9 m/s was close to the original configuration.

1. Introduction

Internal combustion engines are one of the main causes of carbon dioxide production and green-house effect, responsible of global warming and climatic changes. Solar energy is one of the most considered sources of power among renewable resources [1].

The application of solar energy in the automotive field is currently investigated in researches, mostly regarding racing solar cars [2].

In racing competitions, the total power available from photovoltaic panels is limited. Therefore, the solar vehicles must be as efficient as possible and require research and development of new technologies to be competitive [3].

In addition to safety, aerodynamics and weight are the most important design factors: the vehicle must be as light as possible, with a low center of gravity for maneuverability and have a reduced drag caused by the air resistance. Electric in-wheel motors are often employed. They are permanent magnet three-phase or, less frequently, direct current brushless motors integrated in the wheels, with the advantage of the direct drive and no need for a gearbox and all power losses related to it.

The most indicated and used materials to reduce the overall weight are composite laminates, which allows to reduce the weight and to keep

strong and stiff structural components such as chassis, suspensions, and also non-structural parts like door panels and handles [2].

1.1. Sports solar vehicles safety requirements

Emilia 5 is a 4-seater electric vehicle (Fig. 1), 4500 mm long, 1510 mm wide, and 1230 mm high, powered by photovoltaic panels with 1.1 kW of output, 120 km/h of maximum velocity and a chassis made in CFRP (Carbon Fiber Reinforced Plastic), a strong and light material [4,5] that allows to reduce weight. In fact, the vehicle without passengers weights about 350 kg. It is the fifth model of solar vehicle made by the Onda Solare team, the third in collaboration with the University of Bologna. The previous model, Emilia 4, won several competitions, such as the American Solar Challenge 2018 [6], and gave rise to the study of its CFRP safety cage [7], of the roll cage [8], suspensions [9] and the design and material optimization of the roof [10,11].

The vehicle is designed to participate in the World Solar Challenge (WSC), which is a competition that takes place every two years and consists of crossing Australia from north to south, featuring vehicles designed by students, university researchers and private companies

^{*} Corresponding author.

E-mail address: ana.pavlovic@unibo.it (A. Pavlovic).

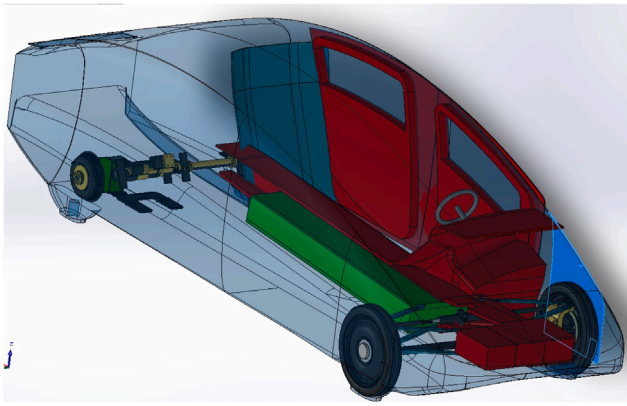


Fig. 1. Model of Emilia 5, solar vehicle made for WSC.

from all over the world [12]. To participate in the competition, it is necessary to demonstrate that the chassis of the vehicle is able to protect the occupants in the event of an impact, by carrying out some finite element simulations [12].

The main purpose of this study is to perform the three crash test simulations on the almost entire vehicle Emilia 5 to verify that the safety requirements of the WSC are met. The simulations are set up and calculated in Ansys LS-Dyna 2023 R1 [13], while the LS-Dyna R13 [14] standalone software is used to generate the seat belts and to measure intrusion inside the cockpit.

Crash simulations are non-linear explicit finite element calculations and require a huge amount of computational resources to be carried out [15,16]. Furthermore, modeling CFRP components adds the extra difficulty of the anisotropy of the material, i.e the mechanical properties change with respect to the orientation of the loads [17]. Therefore, in scientific literature it is rare to find crash tests performed on entire vehicles, with the exception of [5,18]. Crash simulations on composite materials often only concern simple components such as plates submitted to bending impact [19], low velocity impact [20,21], barriers subjected to bullet impact [22] or tubes of various section subjected to axial impact [23–27]. The tests carried out in this study instead, involve the almost entire CFRP vehicle with seat, seatbelts and dummy.

The three impact tests required by the WSC regulations use accelerations as loads, expressed in g (the acceleration of gravity on Earth, 9.81 m/s). The tests are performed as follows [12]:

- frontal impact test: a 5 g load, opposing the direction of travel, applied to the front of the occupant cell in an area less than 250 mm high and less than 600 mm wide.
- side impact test: a 5 g load into the side of the occupant cell, applied adjacent to the driver's torso in an area less than 250 mm high and less than 600 mm wide.
- rollover impact test: a load with components 5 g down, 1.5 g sideways and 4 g backwards, applied at each possible area of contact between the occupant cell and the ground when the occupant cell is upside down.

1.2. EuroNCAP impact simulations

Even if the values of weight and power would make the vehicle fit in the heavy quadricycles [28], the latter can load up to 200 kg of passengers, while Emilia 5 can load up to 320 kg of passengers, reaching the total weight of over 700 kg. Its good aerodynamics also allows it to reach velocities comparable to those of road vehicles. It is therefore not unreasonable that Emilia 5 could be in a situation comparable to the crash tests similar to those to which small road vehicles such as citycars are subjected.

Organizations such as IIHS (Insurance Institute for Highway Safety) in USA [29] and EuroNCAP in Europe [30] carry out various impact

tests in road vehicles, to evaluate their structural integrity and the capacity to protect the passengers. One of the most notorious test is the frontal impact, it consists in giving the vehicle an initial velocity of 64 km/h (17.8 m/s), while the 40% of the front section is aligned with a deformable barrier (40% overlap).

The aftermaths of this test are claimed to be comparable to a collision between 2 vehicles both traveling at 55 km/h (15.5 m/s) [31]. This speed is calculated with the Barrier Equivalent Velocity (BEV) method (more informations about the calculation can be found here [32]). Assuming that the 2 cars are perfectly identical and aligned with a 50% overlap, due to the principle of action and reaction, the forces impressed by one car to the other are equal and opposite and their contact surface would stand still in space, just like the case of a collision against a rigid barrier. Based on this assumption, IIHS successfully carries out crash tests with rigid barriers with resulting deformations similar to those obtained in a collision between two vehicles [33].

The impact test against a rigid barrier at 15.5 m/s with 50% of the front can therefore be considered equivalent to the crash tests carried out at 17.8 m/s against a deformable barrier with 40% overlap, with the advantage that there is no necessity to use computational resources to calculate the deformation of the barrier in FEM crash simulations.

Impact simulations involving 100% and 50% of the front aligned with the rigid barrier are performed in this paper and deformations in the various cases are examined, to have further information about the deformation capacity of the chassis.

Afterwards, by transferring the data relating to the velocity of the vehicle during the impact to a sled test with a seat and a dummy, the accelerations experienced by the dummy's head, Head Injury Criterion (HIC), and contact force between the chest and the belt are compared as the overlap varies.

The HIC is one of the most used parameters to evaluate probability of head injury. It consists in calculating the acceleration integral in a time interval ($t_2 - t_1$) of 15 ms [34], in which the maximum acceleration peak is reached. In finite element modeling of direct head impact [35], the HIC calculated from the head acceleration was found to be generally proportional to the impact force, coup pressure, brain maximum shear stress, and skull von Mises stress [34]. The formula is as follows:

$$\max \left\{ (t_2 - t_1) \left[\frac{1}{t_2 - t_1} \int_{t_1}^{t_2} a(t) dt \right]^{2.5} \right\} \quad (1)$$

The result of Eq. (1) is a number proportional to the probability of suffering head damage. In frontal impact tests, a value of HIC below 700 is considered good in vehicles equipped with airbags [18]. The calculation of the HIC is not required to participate in the WSC, therefore the dummy model does not have to be validated. It is however of interest to compare head accelerations, and chest loads in frontal impact tests with different overlaps, keeping in consideration the fact that the vehicle is not designed to be provided with airbags and to be homologated for road circulation.

1.3. Crash box parametric analysis

More crash simulations are carried out in order to improve the front crash box, whose purpose is the energy absorption in frontal impacts at low velocity. The crashworthiness of the original component, made up of flat plates with a sandwich structure in carbon fabrics and foam, is compared with a crash box created with corrugated laminates composed only of carbon fabrics. In the scientific literature there are several studies about Corrugated Composite Plates (CCPs). Donati and Rondina (2020) investigated the behavior of composite structures in CCP under compressive loading [36].

Ren, Zhang and Xiang (2017) [37], conducted a study about the optimization of a structural component of an aircraft fuselage, by comparing various geometries of the corrugated laminate.

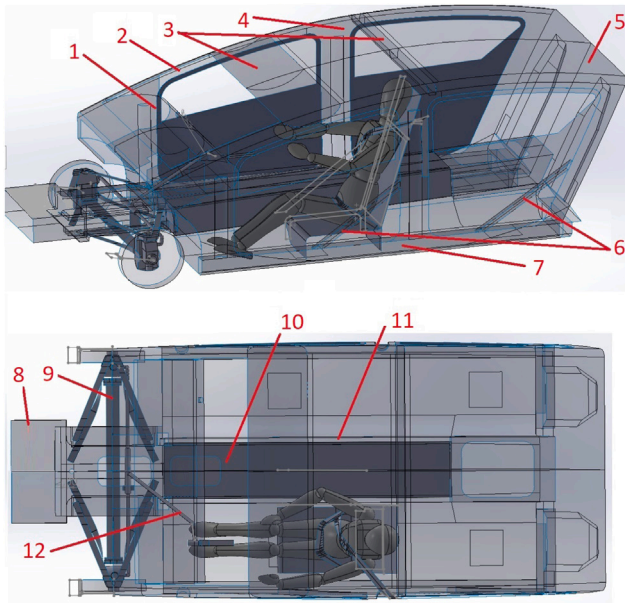


Fig. 2. Main components: (1) Dashboard, (2) Frontal pillar, (3) Roof reinforcement bars, (4) Center pillar, (5) Chassis, (6) Anti-intrusion bars, (7) Side sill, (8) Crash box, (9) Front axle, (10) Battery, (11) Central chassis member, (12) Steering column.

The same concept of this study is applied to the frontal crash box, re-proposing the wavy profile on a parallelepiped of the same size as the crash box, with the sinusoidal curve applied with different amplitudes. The conditions of a full frontal impact at the velocity of 9 m/s (32 km/h) against a rigid barrier are simulated for each geometry, and the forces and deformations are compared.

The article outline consists of the following:

- Methodology (geometry modeling, FE discretization, contact definition, mechanical properties of materials, mathematical model of materials, laminate stratification, crash box parametric analysis, loads and boundaries).
- Results and discussion (WSC impact simulation, EuroNCAP impact simulation, Crash box parametric analysis).
- Conclusions that will provide readers with a clear overview of the structure of the presented work and what to expect from each section.

2. Methodology

2.1. Geometry modeling

The Emilia 5 development team created a 3D model of the vehicle, including chassis, suspensions and engines (Fig. 1). The first step to set up the simulation environment is to transform the 3D model into a shell body. Several details are eliminated to reduce the calculation time. Only the most important components involved in energy absorption during the impact tests, such as the chassis and front suspensions, are included in the model (Fig. 2). The assembly (Fig. 2) is composed by: Dashboard, Frontal pillar, Roof reinforcement bars, Center pillar, Chassis, Anti-intrusion bars, Side sill, Crash box, Front axle, Battery, Central chassis member, Steering column. The rear axle and the electric motors are replaced by distributed masses applied on the chassis.

The chassis is 3290 mm long, 1510 mm wide, and 1136 mm high, and its weight is around 80 kg. The regenerated shell body model has smoother and simplified surfaces, since details such as suspension links and nervatures are removed. The crash box is located in the frontal part of the chassis, it has a parallelepiped shape, 334 mm long, 632 mm wide and 162 mm high.

The doors (Fig. 3a) consist of a 60 mm wide box, with the anti-intrusion bar, made of a 40 × 40 mm squared section hollow bar in

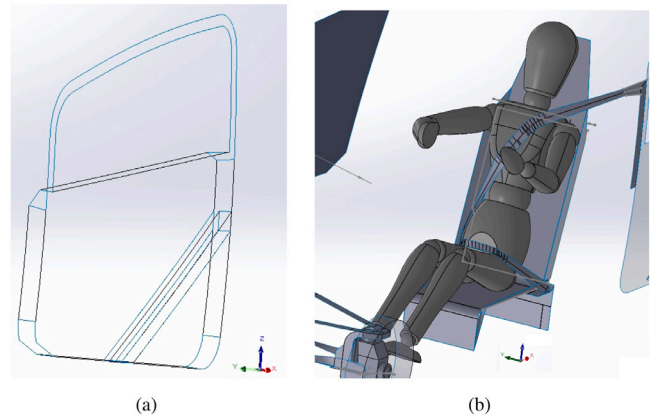


Fig. 3. 3D models: (a) Door with anti-intrusion bar. (b) Seatbelts, seat and dummy.

CFRP. It is connected to the central pillar and to the side sill of the chassis. Its purpose is to protect the occupants in the event of a side impact, preventing the intrusion into the passenger compartment by objects involved in lateral crashes.

The 3-points seat belt approximated model (Fig. 3b) is generated using the dedicated LS-Dyna utility which allows tracing the lines of the belt tangent to the dummy's body and simulating the shape of the band once the preload is applied, so that there is no excessive band length causing inadequate body restraint during impacts (Fig. 3b). The dummy (3D model is available here [38]) is characterized by the size of a man of average weight (70 kg), while the shape of the elongated head simulates the size of the pilot's helmet. The joints that connect the 17 pieces of the dummy have spherical or cylindrical surfaces to facilitate the drawing of their reference coordinates.

The battery is schematized with a parallelepiped having a mass of 150 kg, and it is located under the chassis.

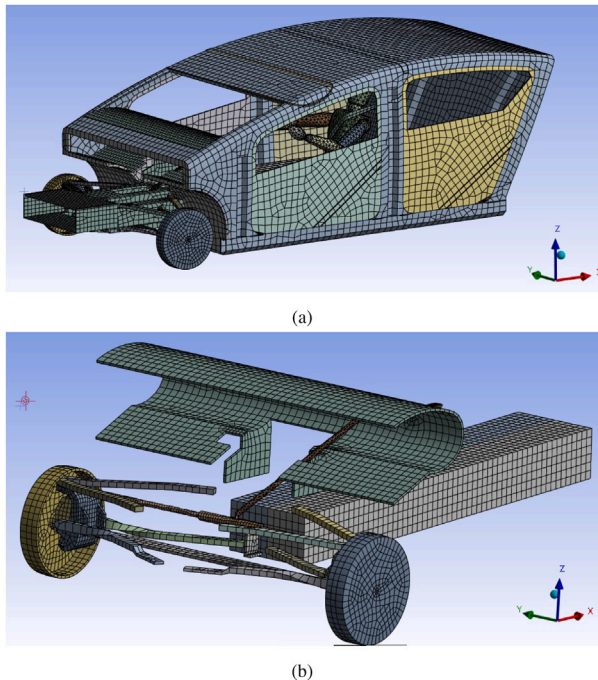
2.2. Finite element discretization

After modeling the components using the CAD software, the assembly (Fig. 2) is imported in Parasolid format in Ansys.

The mesh has to be as rough as possible (Fig. 4a), especially in the areas not affected by significant deformations, to minimize the number of nodes and to have a time step not smaller than $1e-8$ s. The physical preference of the mesh is set as explicit, with linear element order. Shell elements are quadrilaterals, while solid elements are hexahedrons. The maximum size of the elements of the mesh is 50 mm, the *Defeature size* of 5 mm ignores edges and surfaces smaller than the chosen threshold; the *Capture Curvature* function reduces the size of the elements where the surface is curved, while *Capture Proximity* reduces the size of the elements near the edges. In both cases these functions increase the number of nodes without bringing targeted benefits in the areas affected by deformation, then they are deactivated. To make the contact between chassis and doors effective, functions such as *Contact Sizing*, *Node Merging* and *Mesh Connection* are used to match nodes at the interfaces and to have a uniform mesh. For the crash box in the frontal impact, after having carried out several tests to get indications on the calculation time, it is possible to reduce elements to 35 mm for the crash box and 40 mm for the front portion of the frame where the suspensions are linked, in order to increase the accuracy of the simulation locally in the areas affected by the deformation without affecting the calculation time. The mesh size of the smaller components of suspensions is 20 mm (Fig. 4b). After meshing, the total number of nodes of the model is 29 665, while the finite elements are 47 732. Table 1 resumes some aspects of element quality of the mesh of the chassis. The quality metric is proportional with the ratio of the volume to the sum of the squares of the edge

Table 1

| Mesh element quality. | |
|------------------------------------|-------|
| Minimum element quality | 0.093 |
| Average element quality | 0.9 |
| Maximum element quality | 0.999 |
| Standard deviation element quality | 0.12 |

**Fig. 4.** Finite element mesh: (a) Mesh of the vehicle. (b) Mesh of suspensions.

lengths for 2D shell elements. The resulting number ranges between 0 (lowest quality, corresponding to elements whose volume is zero or negative) and 1 (highest quality, corresponding to a perfect square or triangle). A high mesh quality grants confidence to the results of the simulations [39]. The minimum element quality suggests that some elements are highly distorted. However, the average element of 0.9 is close to 1, and the standard deviation is of 0.12, so the mesh has an overall good quality, despite the coarse elements.

To make calculation times compatible with the 8 core Desktop PC used to carry out the simulations, several simplifications have to be done. The most important one is the use of a single shell element representing all the layers of the laminate. The number of integration points is chosen equal to the number of layers of the components subjected to deformation. Before carrying out the simulation with the entire model, some preliminary tests are performed with different types of shell elements. The *S/R Co-Rotational Hughes–Liu* shell exhibited a slightly more stable behavior than the *Belytschko–Tsay* formulation, but requires particularly high computational times. The default system, *Belytschko–Tsay*, is preferred because it requires 1/3 of the time to complete the simulation and exhibits a similar behavior.

Is-Dyna standalone software allows the modification of different mesh parameters. Among the most important parameters of the section *Control Shell Parameters*, the *ISTUPD* keyword concerns the thickness variation of the shell bodies. In case of impact tests, this parameter is left deactivated, as the thickness variation can be neglected in thin surfaces, furthermore it is a source of instability and an increase in calculation times. The value of 4 set automatically by Ansys is a recently introduced option [40], with fewer stability problems, which activates the function only for the isotropic elasto-plastic materials present in the model, such as the seat and suspensions. The keyword *LAMSHT* is set as 1 and indicates that the Shell Laminate Theory

is active. This function allows to take into account the fact that the shearing forces are not constant along the thickness of the laminate. If deactivated, the laminates tend to have a too rigid behavior compared to reality [41].

2.3. Contact definition

To mutually constrain vehicle components, bonded contact regions are applied to the appropriate contact surfaces between parts and all relative parameters are set program controlled as default. Frictional contacts are applied in surfaces between dummy, seat and seatbelts, with a static friction coefficient of 0.6 and a dynamic coefficient of 0.4. The frictional contact between the vehicle and the barrier has a static friction coefficient of 0.4 and a dynamic coefficient of 0.2. After making some simulation attempts with various contact models between chassis and the rigid barrier, a more stable behavior emerged, less prone to phenomena such as hourglassing and buckling with a contact model of the *Pure Penalty* type, already used in crash investigations [42]: when a penetration is detected, a force proportional to the depth of the penetration is created by fictitious springs and dampers. It is important that the meshes have similar dimensions if one of the two bodies is rigid, as in this case [40]. For the frictional contact between the chassis and the barrier, the **CONTACT_AUTOMATIC_NODES_TO_SURFACE* is used. It is a one way treatment of contact, meaning that only the user-specified slave nodes are checked for penetration of the master segments [40]. **CONTACT_AUTOMATIC_SURFACE_TO_SURFACE* is used to set the bonded or frictional contacts between non-composite parts. This two-treatment contact is symmetric, it means that both master and slave nodes are checked for penetration, and the definition of the master and slave surface is arbitrary since the results will be the same [40]. For bonded contacts between the composite chassis and other parts, the **CONTACT_TIED_SURFACE_TO_SURFACE_OFFSET* is used. In tied contact types, the slave nodes are constrained to move with the master surface, and an offset distance between the master segment and the slave node is permitted [40]. All values of contact models, remained as default, are shown in Fig. 5.

In the case of the dummy, two different joint configurations are used: fixed and mobile.

Because of software incompatibility, the model of the dummy cannot be provided with springs when combined with material model **MAT_ENHANCED_COMPOSITE_DAMAGE (*MAT_55)*. There remains the possibility of blocking the joints using completely, making the components of the dummy fixed one to each other with keyword **CONSTRAINED_JOINT_LOCKING*. The utility of the dummy with fixed joints is to verify that enough distance is left between the dummy and the interior of the vehicle during the WSC impact tests.

In the sled test there is no **MAT_ENHANCED_COMPOSITE_DAMAGE* material model used, therefore mobile joints combined with springs and dampers can be applied to better simulate human bio-mechanics. Dummy parts and springs are shown in Fig. 6a, while Table 2 resumes the joints and springs used. The keyword **CONSTRAINED_JOINT_REVOLUTE* is used for revolute joints, while **CONSTRAINED_JOINT_SPHERICAL* is used for spherical joints. The utility of the mobile joints configuration is to compare head accelerations in the EuroNCAP simulations. The dummy is not required to participate in the WSC, therefore the dummy model do not have to be validated, condition which would compel to employ more expensive models in terms of computational resources. Values of springs and dampers are chosen arbitrarily in order to obtain limited movement of the head. As for the dummy with fixed joints, the pieces that make up the dummy are rigid bodies, since the calculation of their deformation during the impact would cause an unjustified increase in calculation times, given that the analysis are more focused on vehicle deformation. The configuration implemented for the sled test, is shown in Fig. 6b.

*CONTACT_AUTOMATIC_NODES_TO_SURFACE_(ID/TITLE/MPP)_(THERMAL)

| | | | | | | | | |
|--|-----------|-----------|--------|--------|------------|--------|--------|--------|
| 4 | SSID | MSID | SSTYP | MSTYP | SBOXID | MBOXID | SPR | MPR |
| | 196 | 197 | 2 | 0 | 0 | 0 | 1 | 1 |
| 5 | FS | FD | DC | VC | VDC | FENCHK | BT | DT |
| | 0.4000000 | 0.2000000 | 0.0 | 0.0 | 10.0000000 | 0 | 0.0 | 0.0 |
| 6 | SFS | SFM | SST | MST | SFST | SFMT | ESF | VSF |
| | 0.0 | 0.0 | 0.0 | 0.0 | 0.0 | 0.0 | 0.0 | 0.0 |
| <input type="checkbox"/> Thermal <input type="checkbox"/> T_Friction <input type="checkbox"/> A <input checked="" type="checkbox"/> AB <input type="checkbox"/> ABC <input type="checkbox"/> ABCD <input type="checkbox"/> ABCDE <input type="checkbox"/> ABCDEF | | | | | | | | |
| 9 | SOFT | SOFSC | LCIDAR | MAXPAR | SBOPT | DEPTH | BSORT | FRCFRO |
| | 0 | 0.0 | 0 | 0.0 | 0.0 | 0 | 0 | 0 |
| 10 | PENMAX | THKOPT | SHLTHK | SNLOG | ISYM | JZD3D | SLDTHK | SLDSTF |
| | 0.0 | 0 | 0 | 0 | 0 | 0 | 0.0 | 0.0 |

(a)

*CONTACT_AUTOMATIC_SURFACE_TO_SURFACE_(ID/TITLE/MPP)_(THERMAL)

| | | | | | | | | |
|--|-----------|-----------|--------|--------|------------|--------|--------|--------|
| 4 | SSID | MSID | SSTYP | MSTYP | SBOXID | MBOXID | SPR | MPR |
| | 168 | 169 | 2 | 0 | 0 | 0 | 1 | 1 |
| 5 | FS | FD | DC | VC | VDC | FENCHK | BT | DT |
| | 0.4000000 | 0.2000000 | 0.0 | 0.0 | 10.0000000 | 0 | 0.0 | 0.0 |
| 6 | SFS | SFM | SST | MST | SFST | SFMT | ESF | VSF |
| | 0.0 | 0.0 | 0.0 | 0.0 | 0.0 | 0.0 | 0.0 | 0.0 |
| <input type="checkbox"/> Thermal <input type="checkbox"/> T_Friction <input type="checkbox"/> A <input checked="" type="checkbox"/> AB <input type="checkbox"/> ABC <input type="checkbox"/> ABCD <input type="checkbox"/> ABCDE <input type="checkbox"/> ABCDEF | | | | | | | | |
| 9 | SOFT | SOFSC | LCIDAR | MAXPAR | SBOPT | DEPTH | BSORT | FRCFRO |
| | 2 | 0.0 | 0 | 0.0 | 3.0 | 5 | 0 | 0 |
| 10 | PENMAX | THKOPT | SHLTHK | SNLOG | ISYM | JZD3D | SLDTHK | SLDSTF |
| | 0.0 | 0 | 0 | 0 | 0 | 0 | 0.0 | 0.0 |

(b)

*CONTACT_TIED_SURFACE_TO_SURFACE_OFFSET_(ID/TITLE/MPP)_(THERMAL)

| | | | | | | | | |
|--|--------|--------|------------|------------|------------|--------|--------|--------|
| 4 | SSID | MSID | SSTYP | MSTYP | SBOXID | MBOXID | SPR | MPR |
| | 90 | 91 | 0 | 0 | 0 | 0 | 1 | 1 |
| 5 | FS | FD | DC | VC | VDC | FENCHK | BT | DT |
| | 0.0 | 0.0 | 0.0 | 0.0 | 10.0000000 | 0 | 0.0 | 0.0 |
| 6 | SFS | SFM | SST | MST | SFST | SFMT | ESF | VSF |
| | 0.0 | 0.0 | -8.333e-05 | -8.333e-05 | 0.0 | 0.0 | 0.0 | 0.0 |
| <input type="checkbox"/> Thermal <input type="checkbox"/> T_Friction <input type="checkbox"/> A <input checked="" type="checkbox"/> AB <input type="checkbox"/> ABC <input type="checkbox"/> ABCD <input type="checkbox"/> ABCDE <input type="checkbox"/> ABCDEF | | | | | | | | |
| 9 | SOFT | SOFSC | LCIDAR | MAXPAR | SBOPT | DEPTH | BSORT | FRCFRO |
| | 0 | 0.0 | 0 | 0.0 | 3.0 | 5 | 0 | 0 |
| 10 | PENMAX | THKOPT | SHLTHK | SNLOG | ISYM | JZD3D | SLDTHK | SLDSTF |
| | 0.0 | 0 | 0 | 0 | 0 | 0 | 0.0 | 0.0 |

(c)

Fig. 5. Parameters set in contact models: (a) *CONTACT_AUTOMATIC_NODES_TO_SURFACE. (b) *CONTACT_AUTOMATIC_SURFACE_TO_SURFACE. (c) *CONTACT_TIED_SURFACE_TO_SURFACE_OFFSET.

2.4. Mechanical properties of materials

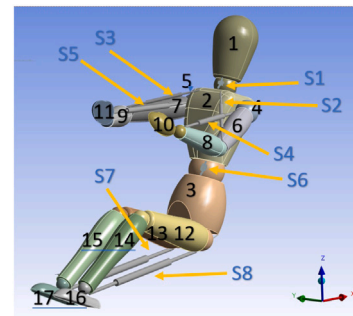
As CFRPs, two different types of fabrics from the Toray product catalog are used in the simulations [43]: To make doors and sandwich structures of the chassis, T700S 12K Plainwave (PW) is used. It is a plain-weave bidirectional prepreg fabric, with a similar number of warp and weft fibers to have similar mechanical properties in 0° and 90° directions (Table 3). To make reinforced components, such as anti-intrusion bars and center pillars, T800S-24K UD, a unidirectional fabric, is used. The absence of warp fibers and the shearing action they cause to weft fibers in bidirectional fabrics, allows to make the most of the mechanical properties in fiber direction (Table 3).

For the majority of sandwich structures, Nomex Aramid Honeycomb with similar properties to ANA-3.2-29 [44] is used. It is an orthotropic material, characterized by low mechanical properties (Table 4), especially in the plane of the cells. For the sandwich structure of the crash box, a polymeric foam is used. Foam is an isotropic material, with low mechanical properties in all directions. The mechanical properties, in Table 5, are similar to Airex T90.100 material [45]. For the suspensions, wheels and seats, made in CFRP, the components can be represented by a fictitious isotropic elastic material ($E = 79 \text{ GPa}$, $\nu = 0.33$, $\rho = 1700 \text{ kg/m}^3$) in order to reduce calculation times. The seatbelts are made of polyethylene (Table 6). An elastic isotropic material is used

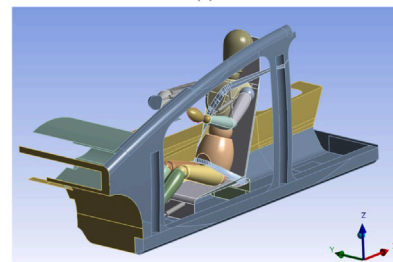
Table 2
Joints and springs of the dummy.

| Joint | Parts connected | Constrain |
|-------|-----------------|------------|
| J1 | 1–2 | Spherical |
| J2 | 2–3 | Spherical |
| J3 | 2–4 | Fixed |
| J4 | 2–5 | Fixed |
| J5 | 4–6 | Spherical |
| J6 | 5–7 | Spherical |
| J7 | 6–8 | Rotational |
| J8 | 7–9 | Rotational |
| J9 | 8–10 | Fixed |
| J10 | 9–11 | Fixed |
| J11 | 3–12 | Spherical |
| J12 | 3–13 | Spherical |
| J13 | 12–14 | Rotational |
| J14 | 13–15 | Rotational |
| J15 | 14–16 | Fixed |
| J16 | 15–17 | Fixed |

| Spring-damper | Parts connected | Stiffness [N/mm] | Damping [N/mm*s] |
|---------------|-----------------|------------------|------------------|
| S1 | 1–2 | 110 | 2 |
| S2 | 2–6 | 150 | 2 |
| S3 | 2–7 | 150 | 2 |
| S4 | 4–10 | 0.4 | 0.8 |
| S5 | 5–11 | 0.4 | 0.8 |
| S6 | 2–3 | 110 | 2 |
| S7 | 3–16 | 0.5 | 0.8 |
| S8 | 3–17 | 0.5 | 0.8 |



(a)



(b)

Fig. 6. Dummy with mobile joints: (a) Dummy parts and springs. (b) Sled test layout.

for the battery ($E = 79 \text{ GPa}$, $\nu = 0.3$, $\rho = 1200 \text{ kg/m}^3$) and the barriers ($E = 200 \text{ GPa}$, $\nu = 0.3$, $\rho = 2850 \text{ kg/m}^3$).

2.5. Mathematical model of materials

For the components of composite materials such as carbon fiber, honeycomb and foam, the material mathematical model used in LS-Dyna is *MAT_ENHANCED_COMPOSITE_DAMAGE (*MAT_55), an enhanced version of *MAT_22. It differs from *MAT_54 for the Tsai-Wu failure criterion [47]. *MAT_54/55 are the most used material models in composite applications [48,49]. Unfortunately, the Ansys LS-DYNA manual does not contain detailed definitions of the input parameters

Table 3
Mechanical properties of carbon fabrics [43].

| | Units | T700S-PW | T800S-UD |
|--------------------------------------|-------------------|----------|----------|
| 0° Tensile strength (X_t) | MPa | 1089 | 2792 |
| 90° Tensile strength (Y_t) | MPa | 993 | 51 |
| 0° Tensile modulus (E_{1t}) | GPa | 59.2 | 145 |
| 90° Tensile modulus (E_{2t}) | GPa | 56.7 | 9 |
| 0° Compressive strength (X_c) | MPa | 674 | 1241 |
| 90° Compressive strength (Y_c) | MPa | 638 | 221 |
| 0° Compressive modulus (E_{1c}) | GPa | 53.3 | 24 |
| 90° Compressive modulus (E_{2c}) | GPa | 48.5 | 9 |
| In-plane shear strength (S_t) | MPa | 86.2 | 90.3 |
| In-plane shear modulus (G_{12}) | GPa | 4.01 | 3.8 |
| Poisson's Ratio | | 0.054 | 0.054 |
| Laminate Density | kg/m ³ | 1510 | 1540 |
| DFAILT | | 0.0184 | 0.0193 |
| DFAILC | | 0.0139 | 0.138 |
| DFAILM | | 0.0178 | 0.005 |
| DFAILS | | 0.02 | 0.023 |

Table 4
Mechanical properties of Honeycomb [7,44].

| | Units | Aramid Honeycomb |
|--------------------|-------------------|------------------|
| Young modulus xy | MPa | 60 |
| Young modulus yz | MPa | 255 |
| Shear modulus xy | MPa | 15 |
| Shear modulus yz | GPa | 35 |
| Poisson's ratio xy | | 0.049 |
| Poisson's ratio xz | | 0.001 |
| Density | kg/m ³ | 80 |

Table 5
Mechanical properties of foam [45].

| | Units | Foam |
|----------------------|-------------------|------|
| Compressive strength | MPa | 60 |
| Compressive modulus | MPa | 1.4 |
| Tensile strength | MPa | 2.2 |
| Tensile modulus | MPa | 120 |
| Shear strength | MPa | 0.8 |
| Shear modulus | MPa | 20 |
| Density | kg/m ³ | 110 |

Table 6
Mechanical properties of polyethylene [46].

| | Units | Polyethylene |
|-----------------|-------------------|--------------|
| Young modulus | MPa | 3000 |
| Poisson's ratio | | 0.42 |
| Bulk modulus | MPa | 6000 |
| Shear modulus | MPa | 1000 |
| Density | kg/m ³ | 950 |

used. (*MAT_55) consists of failure strain parameters such as the maximum strain for fiber tension in fiber direction (DFAILT), compressive failure strain (DFAILC), maximum strain for matrix straining in tension or compression (DFAILM) and shear strain failure (DFAILS). These parameters can be defined as follows [50]:

$$DFAILT = \frac{X_t}{E_{1t}} \tag{2}$$

$$DFAILC = \frac{X_c}{E_{2c}} \tag{3}$$

$$DFAILM = \frac{y_t}{E_{2t}} \tag{4}$$

$$DFAILS = \frac{S_c}{G_{12}} \tag{5}$$

*MAT_026_HONEYCOMB and *MAT_CRUSHABLE_FOAM would be more suitable to model honeycomb and foam [51], however, they are not implemented in Ansys LS-Dyna 2023 R1, therefore, MAT_55 is used

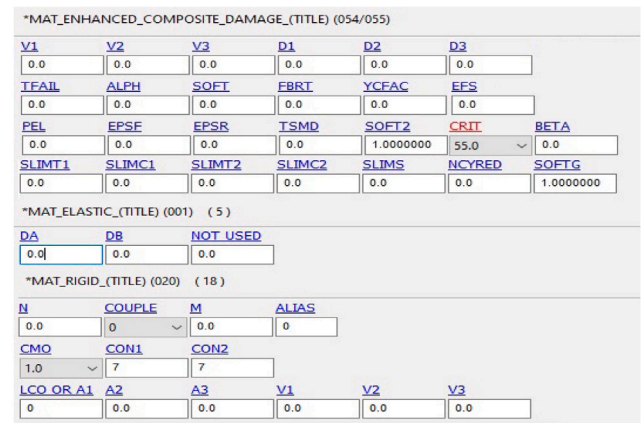


Fig. 7. Material model parameters set as default.

to represent all sandwich structure materials. The material mathematical model used for isotropic materials is *MAT_ELASTIC (*MAT_001). This model is used to describe mechanical properties of a material in the elastic region of the stress–strain curve [41], like the initial phase of deformation of the material in a crash investigation [52]. *MAT_020_RIGID is applied to the rigid barriers. In *MAT_020_RIGID, rigid elements are bypassed in the element processing and no storage is allocated for storing history variables in the process calculation. Therefore, the rigid material type is very cost efficient [41]. All remaining parameters of material models are set as default and are presented in Fig. 7

2.6. Laminate stratification

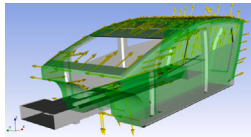
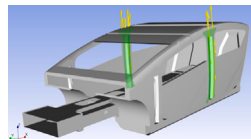
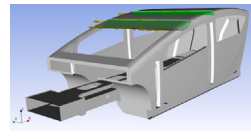
The Emilia5 monocoque chassis, entirely made in CFRP, features carbon fiber roof reinforcing bars and reinforced center pillars. An Ansys Composite Prepost (ACP) block is used to set the layers of the laminates that make up the vehicle's chassis and doors. A sandwich structure is used for the passenger compartment, which is the main part of the chassis, featuring two carbon layers of 2 mm of thickness, separated by 12 mm of honeycomb, for a total thickness of 16 mm. The carbon fabrics used are plain weave (woven), arranged at various angles, symmetrically from the center. The crash box involves the same sequence of carbon fabrics used for the chassis, while 5 mm of foam are used instead of honeycomb. The crash boxes with corrugated geometry are made of the same carbon layers of the chassis, with no core material employed. Material orientation and stratification of components are shown in Table 7

Mostly unidirectional high-strength fibers are used in the direction of the pillar, in order to strengthen it to guarantee the survival space in the event of a side impact and rollover. The total thickness is 11 mm (in Table 7 the stratification layout). In reinforcing elements of roof, the laminate is composed of 7 mm of almost completely unidirectional fibers (Table 7), oriented along the axis of the bars. The box that constitutes the main part of the door is 2 mm thick and it is made of bidirectional fabrics, while the anti-intrusion bar is mostly made of unidirectional fibers oriented along the bar, with a total thickness of 5 mm (Table 7).

2.7. Crash box parametric analysis setup

In this test, the original configuration of the frontal crash box (Fig. 8a), made up with planar surfaces, is compared with crash boxes made by corrugated geometry: the wavy panels are used to make a

Table 7
Part properties.

| Part | Material and layup | Layup | | |
|---|--------------------|----------------------|-------|----------------|
| | | Fabric | Angle | Thickness [mm] |
| | | | | |
| Passenger compartment  | | T700S-PW | 0 | 0.8 |
| | | T700S-PW | 45 | 0.4 |
| | | T700S-PW | -45 | 0.4 |
| | | T700S-PW | 90 | 0.4 |
| | | Honeycomb | 0 | 12 |
| | | T700S-PW | 90 | 0.4 |
| | | T700S-PW | -45 | 0.4 |
| | | T700S-PW | 45 | 0.4 |
| | | T700S-PW | 0 | 0.8 |
| | | Total thickness [mm] | 16 | |
| | Weight [kg] | 70 | | |
| | Material model | *MAT 55 | | |
| Center pillar  | | | | |
| | | T700S-PW | 0 | 0.4 |
| | | T800S-UD | 0 | 0.8 |
| | | T800S-UD | 0 | 0.4 |
| | | T800S-UD | 0 | 0.4 |
| | | Honeycomb | 0 | 7 |
| | | T800S-UD | 0 | 0.4 |
| | | T800S-UD | 0 | 0.4 |
| | | T800S-UD | 0 | 0.8 |
| | | T700S-PW | 0 | 0.4 |
| | Thickness [mm] | 11 | | |
| | Weight [kg] | 2 | | |
| | Material model | *MAT 55 | | |
| Roof reinforcements  | | | | |
| | | T700S-PW | 0 | 0.4 |
| | | T800S-UD | 0 | 1 |
| | | T800S-UD | 0 | 1 |
| | | T800S-UD | 0 | 1 |
| | | T800S-UD | 90 | 0.4 |
| | | T800S-UD | 0 | 1 |
| | | T800S-UD | 0 | 1 |
| | | T800S-UD | 0 | 1 |
| | | T700S-PW | 0 | 0.4 |
| | Thickness [mm] | 7.2 | | |
| | Weight [kg] | 9.6 | | |
| | Material model | *MAT 55 | | |

(continued on next page)

parallelepiped with the same dimensions of the standard front crash box. The sinusoidal profile of the panels is obtained with the following equation:

$$y = A * \sin(x * 2 * \pi / 60) \tag{6}$$

The wavelength of the sinusoidal profile is 60 mm. The values 4, 6 and 13 mm (Fig. 8b, c, d respectively) are used for the sinusoidal semi-amplitude A. The rear panel of the corrugated geometry is connected, using a bonded contact, to a solid body with the same mathematical model and mechanical properties of the battery, except for the total mass of 800 kg representing the vehicle. The test compares different amplitudes of sinusoidal geometry in a simulation of a frontal impact of the vehicle at the velocity of 9 m/s against a rigid barrier. The size of the mesh is 10 mm in order to be able to represent the curvature of the sinusoidal profile with adequate accuracy.

2.8. Loads and boundaries

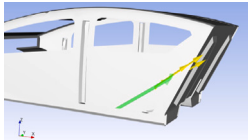
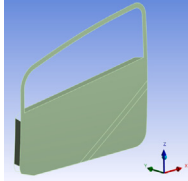
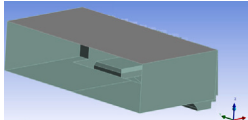
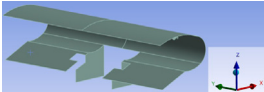
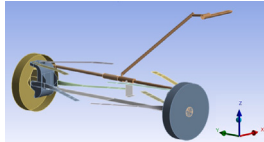
For the WSC impacts, accelerations are applied to the vehicle and the dummy, according to the regulations. To be conservative, in addition to the total mass of the vehicle increased to 800 kg including passengers, against the approximately 700 kg of the actual vehicle, the gravitational acceleration is rounded up to $g = 10 \text{ m/s}^2$ to set the loads. For the frontal impact, the initial velocity is applied instead of the acceleration. In both cases, the rigid barriers are fixed in space by applying the *Fixed support* boundary. Table 8 resumes the loads of all simulations.

3. Results and discussion

3.1. WSC impact simulations

Frontal impact

Table 7 (continued).

| | | | | |
|---------------------|---|----------------|----------|----------------|
| Anti-intrusion bars |  | Layup | | |
| | | Fabric | Angle | Thickness [mm] |
| | | T700S-PW | 0 | 0.4 |
| | | T800S-UD | 0 | 1 |
| | | T800S-UD | 0 | 1 |
| | | T800S-UD | 90 | 0.4 |
| | | T800S-UD | 0 | 1 |
| | | T800S-UD | 0 | 1 |
| T700S-PW | 0 | 0.4 | | |
| Thickness [mm] | 5.2 | | | |
| Weight [kg] | 0.8x4 | | | |
| Material model | *MAT 55 | | | |
| Doors |  | Layup | | |
| | | Fabric | Angle | Thickness [mm] |
| | | T800S-UD | 0 | 0.4 |
| | | T800S-UD | 45 | 0.4 |
| | | T800S-UD | -45 | 0.4 |
| | | T800S-UD | 45 | 0.4 |
| | | T800S-UD | 0 | 0.4 |
| | | Thickness [mm] | 2 | |
| Weight [kg] | 3.5x4 | | | |
| Material model | *MAT 55 | | | |
| Crash box |  | Layup | | |
| | | Fabric | Angle | Thickness [mm] |
| | | T700S-PW | 0 | 0.8 |
| | | T700S-PW | 45 | 0.4 |
| | | T700S-PW | -45 | 0.4 |
| | | T700S-PW | 90 | 0.4 |
| | | Foam | 0 | 5 |
| | | T700S-PW | 90 | 0.4 |
| | | T700S-PW | -45 | 0.4 |
| | | T700S-PW | 45 | 0.4 |
| | | T700S-PW | 0 | 0.8 |
| | | Thickness [mm] | 9 | |
| Weight [kg] | 2.5 | | | |
| Material model | *MAT 55 | | | |
| Dashboard |  | Thickness [mm] | 5 | |
| | | Weight [kg] | 15 | |
| | | Material | CFRP | |
| | | Material model | *MAT 001 | |
| Front axle |  | Thickness [mm] | 10 | |
| | | Weight [kg] | 32 | |
| | | Material | CFRP | |
| | | Material model | *MAT 001 | |

(continued on next page)

The simulation (Fig. 9) terminates after calculating 0.18 s from the application of the load. At this time, the minimum of kinetic energy is already reached and the impact event can be considered over. Following the application of the load (5 g in x direction) the vehicle is pushed against the rigid barrier.

Upon the application of acceleration of 5 g along the driving direction (x axis), the front section of the crash box, engineered with reduced mechanical properties to effectively absorb shocks at lower velocities, undergoes collapse. This collapse results in a rapid acceleration of the vehicle bodies (measured at the base of the seat, with a sample frequency of 1000 Hz and filtered at 300 Hz), from 0 m/s to 3.92 m/s (Fig. 10). By approximately 0.115 s, after absorbing 8531 J of energy, the crash box has fully collapsed, initiating contact between the barrier and the sturdier material positioned behind it. This interaction triggers a significant deceleration event, surpassing 30 g for 2 ms, with a peak

of 55 g recorded at 0.145 s (Fig. 10). By 0.147 s, the vehicle has ceased all forward motion, having attained the maximum accumulation of internal energy, measured at 9826 J (Fig. 11). Subsequently, while the most part of internal energy is spent in composite failure, a smaller amount is converted in kinetic energy (Fig. 11), resulting in the vehicle rebounding. The maximum linear displacement observed in the chassis is recorded at 333 mm (Fig. 9), marking the pinnacle of deformation during the crash sequence.

The hourglass energy remains below 10% of the internal energy, while the contact energy, as expected from sliding between surfaces with frictional contact, returns positive values. The energy balance of the simulation suggests that parameters have been set correctly. The passenger compartment is not affected by significant deformations. The relative distance between the front and center pillar undergoes variations of tenths of millimeter, caused by the vibration of the chassis in

Table 7 (continued).

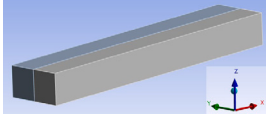
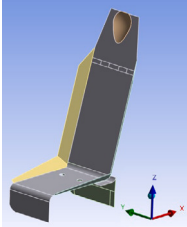
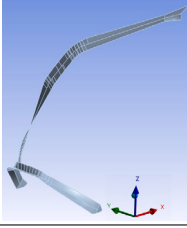
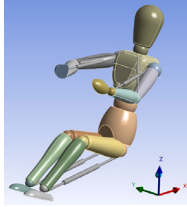
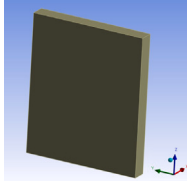
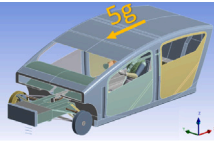
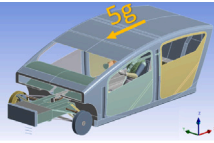
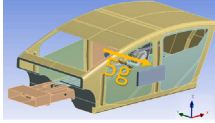
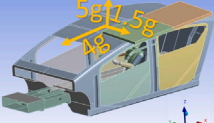
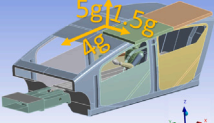

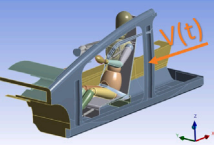
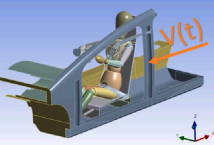
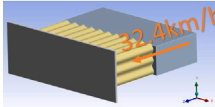
| | | | | | | | | | | |
|----------------|--|--|----------------|------|-------------|--------------|----------------|--------------|----------------|----------|
| Battery |  | <table border="1"> <tr> <td>Weight [kg]</td> <td>150</td> </tr> <tr> <td>Material</td> <td>Lithium</td> </tr> <tr> <td>Material model</td> <td>*MAT 001</td> </tr> </table> | Weight [kg] | 150 | Material | Lithium | Material model | *MAT 001 | | |
| Weight [kg] | 150 | | | | | | | | | |
| Material | Lithium | | | | | | | | | |
| Material model | *MAT 001 | | | | | | | | | |
| Seat |  | <table border="1"> <tr> <td>Thickness [mm]</td> <td>5 mm</td> </tr> <tr> <td>Weight [kg]</td> <td>5</td> </tr> <tr> <td>Material</td> <td>CFRP</td> </tr> <tr> <td>Material model</td> <td>*MAT 001</td> </tr> </table> | Thickness [mm] | 5 mm | Weight [kg] | 5 | Material | CFRP | Material model | *MAT 001 |
| Thickness [mm] | 5 mm | | | | | | | | | |
| Weight [kg] | 5 | | | | | | | | | |
| Material | CFRP | | | | | | | | | |
| Material model | *MAT 001 | | | | | | | | | |
| Seatbelt |  | <table border="1"> <tr> <td>Thickness [mm]</td> <td>0.8</td> </tr> <tr> <td>Weight [kg]</td> <td>0.2</td> </tr> <tr> <td>Material</td> <td>Polyethylene</td> </tr> <tr> <td>Material model</td> <td>*MAT 001</td> </tr> </table> | Thickness [mm] | 0.8 | Weight [kg] | 0.2 | Material | Polyethylene | Material model | *MAT 001 |
| Thickness [mm] | 0.8 | | | | | | | | | |
| Weight [kg] | 0.2 | | | | | | | | | |
| Material | Polyethylene | | | | | | | | | |
| Material model | *MAT 001 | | | | | | | | | |
| Dummy |  | <table border="1"> <tr> <td>Weight [kg]</td> <td>70</td> </tr> <tr> <td>Material</td> <td>Polyethylene</td> </tr> <tr> <td>Material model</td> <td>*MAT 020</td> </tr> </table> | Weight [kg] | 70 | Material | Polyethylene | Material model | *MAT 020 | | |
| Weight [kg] | 70 | | | | | | | | | |
| Material | Polyethylene | | | | | | | | | |
| Material model | *MAT 020 | | | | | | | | | |
| Barriers |  | <table border="1"> <tr> <td>Weight [kg]</td> <td>0</td> </tr> <tr> <td>Material</td> <td>Steel</td> </tr> <tr> <td>Material model</td> <td>*MAT 020</td> </tr> </table> | Weight [kg] | 0 | Material | Steel | Material model | *MAT 020 | | |
| Weight [kg] | 0 | | | | | | | | | |
| Material | Steel | | | | | | | | | |
| Material model | *MAT 020 | | | | | | | | | |

Table 8 Applied loads.

| | Simulation | Loads | Simulation | Loads |
|---------------------|---|---|--|--|
| WSC Frontal impact |  |  | WSC lateral impact |  |
| WSC rollover impact |  |  | Frontal impact with 50% and 100% overlap |  |
| Dummy analysis |  |  | Parametric analysis |  |

the impact. As a result, the survival space in the passenger compartment is not affected in this simulation.

Side impact

Following the application of the acceleration in the transverse direction, the vehicle is pushed against the rigid barrier in the left side. The

center pillar is the component which absorbs the most of the internal energy (2618 J).

The maximum shear stress of 262 MPa (Fig. 12) is reached in the center pillar. This value is above the shear strength of unidirectional fibers, which is 90 MPa. The maximum principal stress of 510 MPa

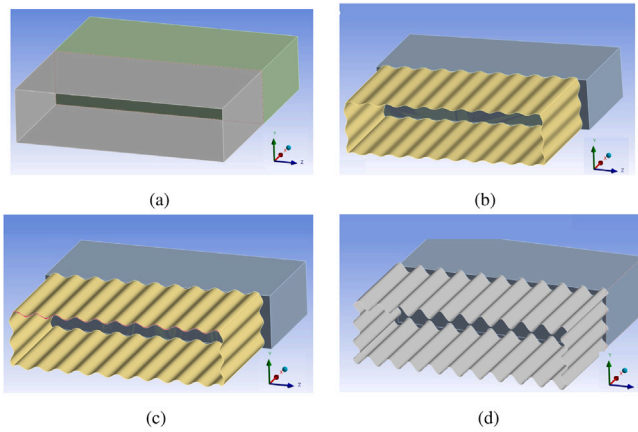


Fig. 8. Geometries of the crash box and the solid body: (a) Standard configuration, (b) Sinusoid semi-amplitude $A = 4$ mm, (c) Sinusoid semi-amplitude $A = 6$ mm, (d) Sinusoid semi-amplitude $A = 13$ mm.

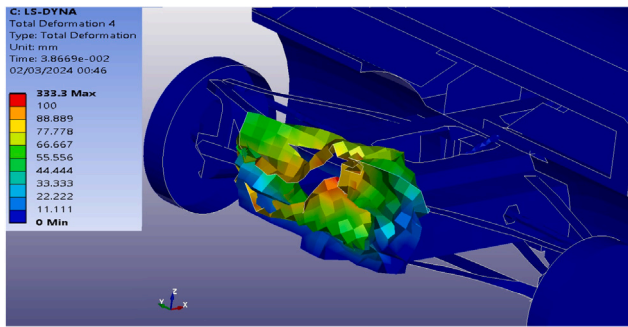


Fig. 9. Linear displacement of the vehicle in frontal impact analysis.

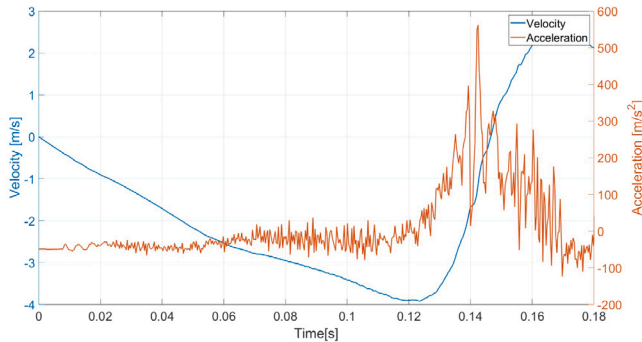


Fig. 10. Velocity and acceleration curves of the vehicle in frontal impact.

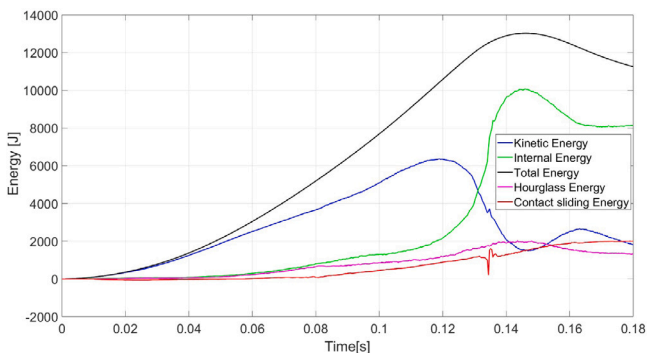


Fig. 11. Energy curves in WSC frontal impact.

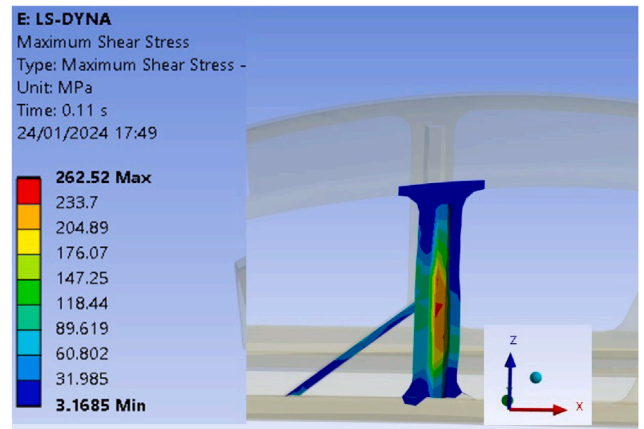


Fig. 12. Distribution of the maximum shear stress in the center pillar and anti-intrusion bar in side impact.

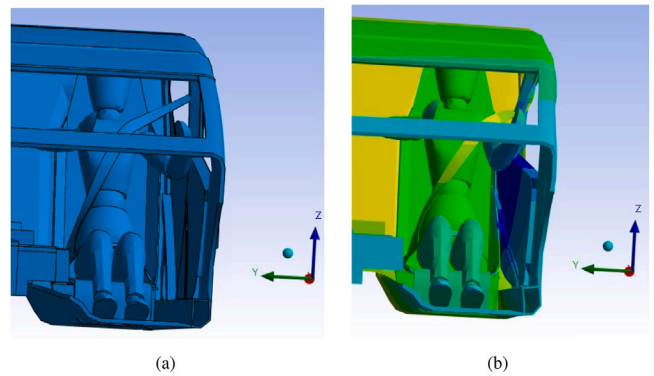


Fig. 13. Intrusion inside the cabin: (a) Survival space before the application of load. (b) Anti-intrusion bar in contact with the seat after load application.

(compressive strength of material is around 700 MPa) is reached in the same spot.

The seat, before the impact, has a minimum distance from the anti-intrusion bar of 112 mm (Fig. 13a). The maximum intrusion into the cabin is measured, in proximity of the anti-intrusion bar in the door, where the maximum displacement is of 160 mm. This is a significant deformation which causes the door to penetrate in the seat area approximately 50 mm deep. However, the survival space still remains within the regulations limits (Fig. 13b).

Rollover

The accelerations imposed by the regulations in the three components are applied, pushing the roof of the vehicle against the rigid barrier. The maximum shear stress of 95 MPa is reached in the center pillar and in the roof reinforcement bar (Fig. 14), a value slightly above the shear strength of unidirectional fibers which is 90 MPa. The maximum directional stress of 162 MPa is reached in the roof reinforcement bar, the value remains below the compressive strength of 1000 MPa. The roof absorbs 2338 J of energy.

The maximum displacement between a point above the driver's head in the roof and the vehicle floor is lower than 25 mm. Therefore, the survival space in the cockpit remains sufficient, and the roof does not touch the head of the dummy, which has an initial minimum distance between the roof of 50 mm. In summarizing the results concerning WSC simulations, across three tests, the vehicle demonstrated commendable behavior with no significant deformations observed in the passenger compartment that would jeopardize survival space. By refining the mesh and reducing termination time in simulations (necessary due to constraints posed by available computational

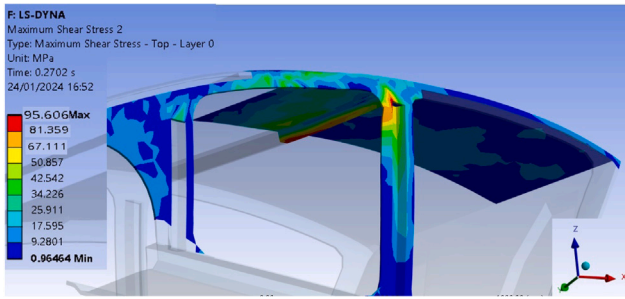


Fig. 14. Shear stress in rollover impact.

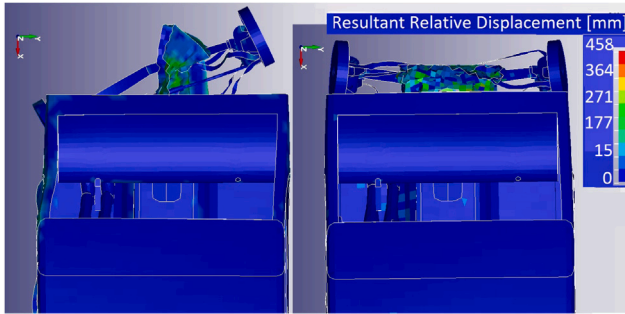


Fig. 15. Frontal impact with 100% and 50% overlap.

resources), the chassis exhibited comparable behavior. This implies that despite the coarse mesh, the results are converging with satisfactory accuracy. Furthermore, in similar crash investigation studies, simulations with shell elements gave results similar to those obtained with solid bodies, in which also delamination is simulated [15].

3.2. EuroNCAP impact simulations

Impact tests are carried out involving 100% and 50% of the frontal section (Fig. 15) against a rigid barrier and deformations are examined in the various cases. The initial velocity of the vehicle is of 15.5 m/s.

Impact test with 100% and 50% overlap.

In the 100% overlap simulation, the crash box absorbs energy and reduces the velocity from 15.55 m/s to 12.8 m/s, between 0.016 s and 0.02 s after the crash box complete collapse. The chassis deformation phase begins, causing a decisive deceleration starting from time 0.024 s (blue curve in Fig. 16). The chassis accumulates part of the elastic potential energy which is subsequently released in form of kinetic energy, moving the vehicle away from the barrier. At the instant 0.05 s the vehicle has reached 0 m/s of velocity (Fig. 16), with the minimum of the kinetic energy and the maximum of the internal energy (Fig. 17). In both simulations, the amount of energy absorbed by the crash box and the frontal part of the chassis is about 20 000 J and 40 000 J respectively. The hourglass energy, with a maximum value of 6000 J (Fig. 18), remains below 10% of the internal energy, while sliding energy returns positive values, a sign that the simulation took place with correct parameters. In EuroNCAP simulation, unlike previous ones, there is no external work caused by the application of the acceleration load. Therefore, the total energy, which is the sum of kinetic, internal, contact sliding and hourglass energy, remains constant.

The same type of setup, except for the position of the barrier, is used for the impact test with 50% of the front aligned with the barrier. In this case, a smaller portion of the front is involved in the impact and it must absorb the same kinetic energy, therefore the deformation have to involve a greater longitudinal depth of the chassis. The vehicle stops in a greater space, the same amount of energy is absorbed over a longer

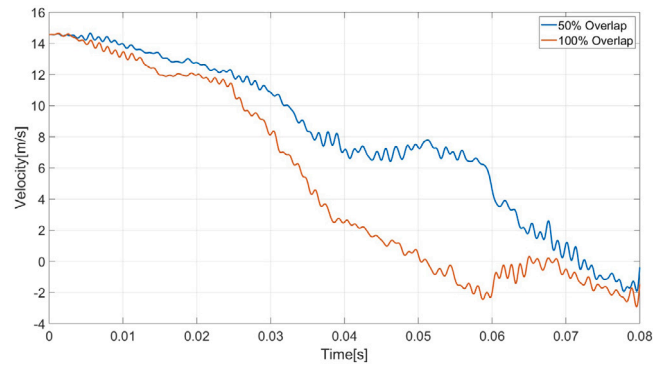


Fig. 16. Velocity curve of the 2 frontal impact tests.

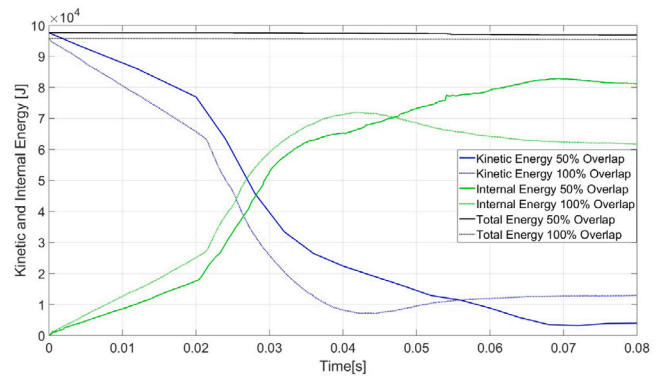


Fig. 17. Kinetic and internal energy curves with overlap at 50% and 100%.

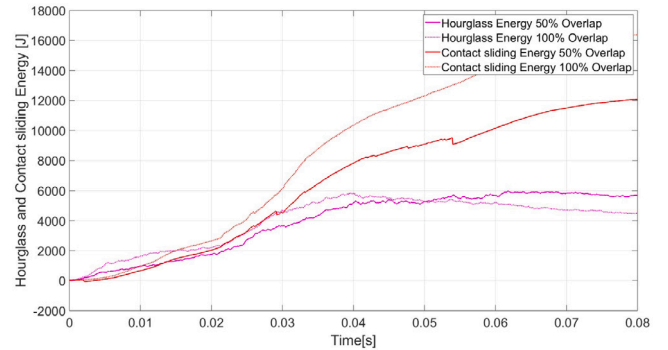


Fig. 18. Hourglass and contact sliding energy curves with overlap at 50% and 100%.

time interval. From the velocity curve in Fig. 16, it can be seen that the accelerations are also lower but they last longer. In the internal energy graphs in Fig. 17, it can be verified that at the second 0.03 the chassis has accumulated 60 000 J of energy in case of 100% overlap, while in case of 50% overlap the chassis has only accumulated 52 000 J. The minimum value of the kinetic energy is reached at a time in which the vehicle velocity reaches 0 m/s, $t = 0.045$ s and 0.07 s for overlap at 100% and 50% respectively. In the subsequent instants the internal energy is released in form of kinetic energy which rises again, and the system regains velocity in the opposite direction. This phenomenon is accentuated to the simulation carried out with parameters of the WSC, due to the greater energies involved and the lack of acceleration load which continues to push the vehicle against the barrier. Furthermore, the higher velocities involved with respect to the WSC simulations, allow to stop the simulation at 0.08 s instead of 0.18 s, because of fact that aftermaths happens in a reduced interval of time. The passenger

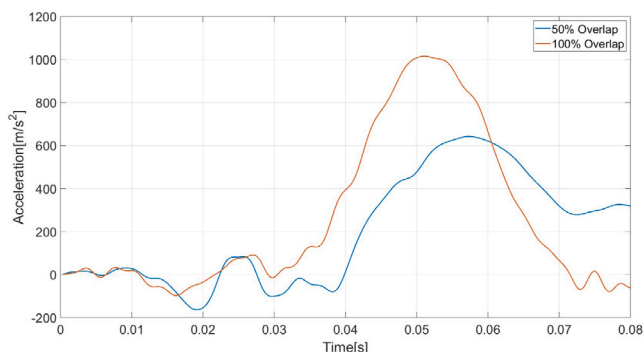


Fig. 19. Acceleration curve of the dummy's head in the frontal impact test with overlap at 100% (a) and 50% (b).

compartment is affected by a slight deformation following the impact of the frontal pillar with the barrier. The shortening of the distance between the frontal pillar and the center pillar is 25 mm in case of an impact with 50% overlap, therefore the survival space is not significantly compromised in these tests.

To calculate stresses on the dummy, the velocity of the frame measured in the previous impact tests is applied to the sled test, with the dummy equipped with mobile joints, springs and dampers. As regards the possibility of damage to the head, the HIC with the accelerations measured on the dummy's head is calculated. The load on the chest, given by contact with the belt during the impact with safety belts with no load limiter, is also measured [53].

Following the application of Eq. (1) with the acceleration obtained from the simulations, the value of HIC scored is 451 in case of a collision with 50% overlap, a value that IIHS would consider acceptable [18], characterized by mild brain concussion and minor skull fracture. The impact with 100% overlap, characterized by an acceleration peak of about 100 g, almost double compared to the 66 g of the impact with 50% overlap (Fig. 19), brings the HIC value over the threshold of acceptability of 700, up to 1239, characterized by severe brain concussion and major skull fracture [18].

Chest accelerations as a parameter to evaluate injuries are not particularly effective, as a low acceleration value of the spine can be indicative of excessive chest deflection with potentially greater damages than those which would occur in the event of higher accelerations and lower deflections [54]. Therefore, no chest acceleration are reported in this paper. Considerations can be made about the load given by the contact between the belt and the chest, peaks of 10 kN (Fig. 20) and 14 kN are measured in the two tests, with 50% and 100% of overlap respectively, while safety belts often have load limiters, not implemented in the simulations. It is still to be determined if the vehicle will have load limiters installed. The maximum load limit is usually 6 kN or 4 kN, a force still causing several fractured ribs but limited organ damage [55]. Without passive safety devices, such as load limiters, which would cause a higher head and chest translation toward the steering wheel, and without airbags limiting accelerations of impacts, head accelerations and chest loads could cause fatal damage in the event of impacts such as those of the homologation tests. No contact between dummy and vehicle interior is observed during the simulations. From the EuroNCAP simulations results, the vehicle structure exhibited a good behavior, especially considering that it is a lightweight vehicle designed for a competition involving low powered engines and low speeds, and it is not meant to be homologated for road circulation or have airbags installed. Because of the lack of seatbelt load limiters and airbags, the head accelerations and chest loads could cause fatal damage in this type of impact.

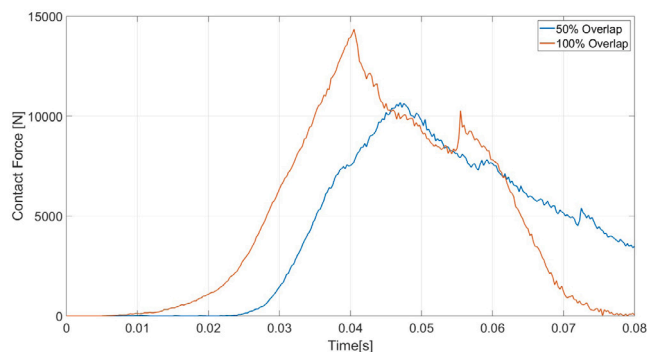


Fig. 20. Load curve given by the chest-belt contact in the impact with overlap at 50%.

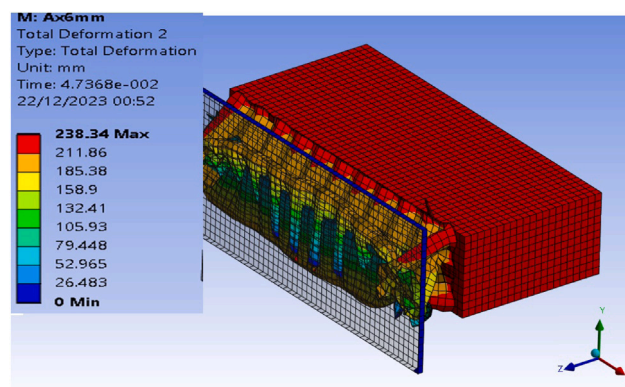


Fig. 21. Simulation of crash box impact.

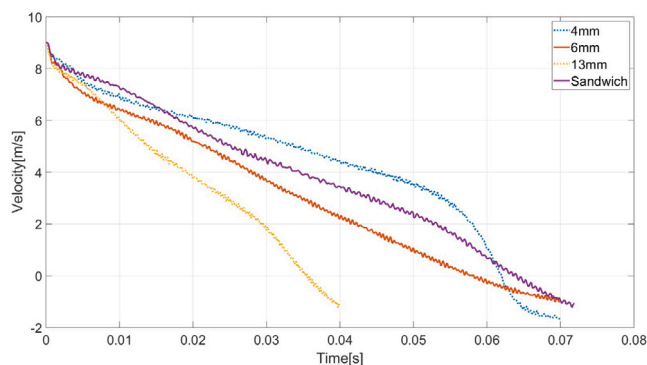


Fig. 22. Velocity curves compared between the original flat sandwich structure and the sinusoidal profiles.

3.3. Crash box parametric analysis

The simulations (Fig. 21) demonstrate that the profile with sinusoidal semi-amplitude $A = 4$ mm is not able to absorb all the impact energy. Fig. 22 shows in blue the rapid decrease in velocity from the instant 0.055 s due to the impact of the block behind the crash box against the rigid barrier in the case with $A = 4$ mm. With $A = 6$ mm the properties are slightly lower than the standard configuration with sandwich structure, while with $A = 13$ mm, the structure is too rigid for a component that should reduce accelerations in low-velocity impacts, exhibiting too little deformation and the highest forces between barrier and crash box.

The CCP plates shows more peaks of force that decrease with deformation. The standard configuration imparts greater strength in the initial instants (Fig. 23), causing longer accelerations. The configuration with no foam and more rounded shape at the edges has

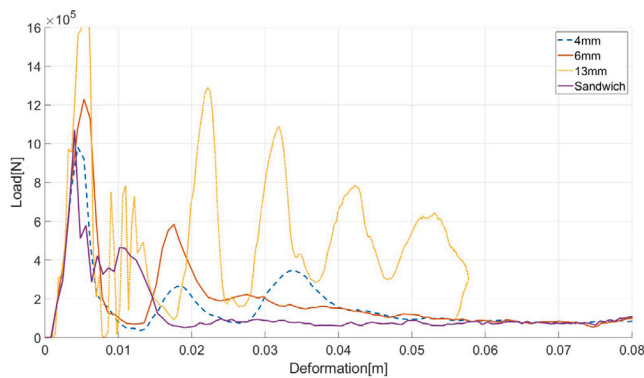


Fig. 23. Curves of the contact force between the crash box and the barrier in comparison between the original flat sandwich structure and the sinusoidal profiles.

more but less durable peaks of acceleration. From the tests, it can be seen that the use of sinusoidal profiles increases the ability to absorb energy in collisions and allows the creation of components that have the same mechanical properties with a smaller quantity of material. With the same reinforcing carbon fiber, in this case, a laminate with a sinusoidal profile with a semi-width (A) of 6 mm exhibits slightly lower properties than those of flat laminates with intermediate foam. From this test emerges the possibility that wider values of A combined with a smaller number of carbon fabric layers are able to obtain lighter and cheaper components with the same functionality. At the moment of the writing of this article, Emilia 5 is still in development phase, therefore, after further considerations about production costs and difficulties, the possibility of using corrugated laminates will be considered.

4. Conclusions

A comprehensive evaluation of the lightweight solar vehicle, CFRP Emilia 5, was conducted to assess its adherence to WSC regulations. Through three crash test simulations utilizing Finite Element Method (FEM) software, as mandated by the competition guidelines, the vehicle demonstrated robust resistance to deformation. Notably, in the frontal impact simulation, the cockpit remained intact. Lateral impact testing revealed a 160 mm intrusion into the cockpit, while the rollover simulation indicated a reduction of 25 mm in the distance between the roof and floor. Importantly, no contact between the internal dummy and the vehicle's interiors was observed across all simulations. From the results of these simulations emerges that the vehicle is able to participate in the WSC competition. To emulate frontal impact tests akin to standard road vehicle approvals, simulations were performed at an initial velocity of 15.5 m/s against a rigid barrier with 100% and 50% overlaps. Results indicated no significant shortening of the distance between the front and center pillar with 100% overlap, while a 25 mm reduction was noted with 50% overlap. Following the crashes, the vehicle's structural integrity remained intact, ensuring sufficient survival space within the cockpit. Subsequent sled testing, incorporating a dummy, seat, seatbelt, and dashboard, utilized the velocity data from the previous simulations. Analysis of head accelerations and chest loads revealed a Head Injury Criterion (HIC) within the safety limit of 700, registering at 451 with 50% overlap, and above the limit at 1239 with 100% overlap. However, chest loads surpassed the approved safety belt limit of 6 kN, recording 10 kN and 14 kN in tests with 50% and 100% overlaps, respectively. From the latter results, the vehicle structure exhibited a good behavior, especially considering that it is a lightweight vehicle designed for a competition involving low powered engines and low speeds, and it is not meant to be homologated for road circulation. Because of the lack of seatbelt load limiters and airbags, the head accelerations and chest loads could cause fatal damage in this type of impact. Additionally,

a comparative study between the original planar sandwich structure of the crash box and one composed of corrugated plates of identical size and layup, without interlayer foam, was conducted. The analysis, varying the semi-amplitude (A) of the sinusoidal profile, indicated that a value of A equal to 6 mm retained energy absorption capabilities close to the original configuration, even under impacts at 9 m/s. This improved configuration allows to build a lighter crash box, with less material. Therefore, after further considerations about production costs, the possibility of using corrugated laminates will be considered. The comparison between different crash box structures, including planar sandwich and corrugated plate configurations, highlights the importance of structural design in energy absorption during crashes. Identifying configurations that improve energy absorption while maintaining structural integrity is crucial for improving overall vehicle safety.

Funding

Financed by the European Union - NextGenerationEU (National Sustainable Mobility Center CN00000023, Italian Ministry of University and Research Decree n. 1033 - 17/06/2022, Spoke 11 -Innovative Materials & Lightweighting). The opinions expressed are those of the authors only and should not be considered as representative of the European Union or the European Commission's official position. Neither the European Union nor the European Commission can be held responsible for them.

CRediT authorship contribution statement

Alessandro Papavassiliou: Writing – original draft, Visualization, Validation, Software, Methodology, Investigation, Formal analysis, Data curation. **Ana Pavlovic:** Writing – review & editing, Writing – original draft, Validation, Supervision, Software, Methodology, Investigation, Formal analysis, Data curation. **Giangiacomo Minak:** Writing – review & editing, Supervision, Resources, Project administration, Methodology, Investigation, Funding acquisition, Conceptualization.

Declaration of competing interest

The authors declare that they have no known competing financial interests or personal relationships that could have appeared to influence the work reported in this paper.

Data availability

Data will be made available on request.

References

- [1] Rizzo G. Automotive applications of Solar Energy. *IFAC Proc Vol* 2010;43(7):174–85. <http://dx.doi.org/10.3182/20100712-3-de-2013.00199>.
- [2] Minak G, Fragassa C, de Camargo FV. A brief review on determinant aspects in energy efficient solar car design and manufacturing. *Sustain Des Manuf* 2017;2017:847–56. http://dx.doi.org/10.1007/978-3-319-57078-5_79.
- [3] Ersöz E. Development of a racing strategy for a solar car (Master's thesis), Middle East Technical University; 2006.
- [4] Fuchs ER, Field FR, Roth R, Kirchain RE. Strategic materials selection in the automobile body: Economic opportunities for polymer composite design. *Compos Sci Technol* 2008;68(9):1989–2002. <http://dx.doi.org/10.1016/j.compscitech.2008.01.015>.
- [5] Minak G, Brugo TM, Fragassa C, Pavlovic A, de Camargo FV, Zavatta N. Structural design and manufacturing of a cruiser class solar vehicle. *J Vis Exp* 2019;(143). <http://dx.doi.org/10.3791/58525>.
- [6] Pavlovic A, Fragassa C, Minak G, Lukovic M. Toward a sustainable mobility: A solar vehicle for a new quality of life. *Proc Eng Sci* 2019;1(2):731–6. <http://dx.doi.org/10.24874/pes01.02.075>.
- [7] Fragassa C, Pavlovic A, Minak G. On the structural behaviour of a CFRP safety cage in a solar powered electric vehicle. *Compos Struct* 2020;252:112698. <http://dx.doi.org/10.1016/j.compstruct.2020.112698>.

- [8] Pavlovic A, Zivkovic M. Roll cage design and validation for a rally vehicle. *FME Trans* 2016;44(4):398–404. <http://dx.doi.org/10.5937/fmet1604398p>.
- [9] De C, Fragassa C, Pavlovic A, Martignani M. Analysis of the suspension design evolution in Solar Cars. *FME Trans* 2017;45(3):394–404. <http://dx.doi.org/10.5937/fmet1703394v>.
- [10] Pavlović A, Sintoni D, Minak G, Fragassa C. On the modal behaviour of ultralight composite sandwich automotive panels. *Compos Struct* 2020;248:112523. <http://dx.doi.org/10.1016/j.compstruct.2020.112523>.
- [11] Pavlovic A, Sintoni D, Fragassa C, Minak G. Multi-objective design optimization of the reinforced composite roof in a solar vehicle. *Appl Sci* 2020;10(8):2665. <http://dx.doi.org/10.3390/app10082665>.
- [12] World solar challenge 2023. 2023, <https://worldsolarchallenge.org/>.
- [13] AnsysInc. Ansys. 2023, URL <https://www.ansys.com>.
- [14] AnsysInc. Ls-Dyna. 2023, URL <https://lsdyna.ansys.com/>.
- [15] Boria S, Obradovic J, Belingardi G. Experimental and numerical investigations of the impact behaviour of composite frontal crash structures. *Composites B* 2015;79:20–7. <http://dx.doi.org/10.1016/j.compositesb.2015.04.016>.
- [16] Le Guenec Y, Brunet J-P, Daim F-Z, Chau M, Tourbier Y. A parametric and non-intrusive reduced order model of car crash simulation. *Comput Methods Appl Mech Engrg* 2018;338:186–207. <http://dx.doi.org/10.1016/j.cma.2018.03.005>.
- [17] Belingardi G, Chiandussi G. Vehicle crashworthiness design — General principles and potentialities of composite material structures. In: Abrate S, editor. *Impact engineering of composite structures*. Vienna: Springer Vienna; 2011, p. 193–264. http://dx.doi.org/10.1007/978-3-7091-0523-8_5.
- [18] Mihradi S, Golfianto H, Mahyuddin AI, Dirgantara T. Head injury analysis of vehicle occupant in frontal crash simulation: Case study of ITB's formula SAE race car. *J Eng Technol Sci* 2017;49(4):534–45. <http://dx.doi.org/10.5614/j.eng.technol.sci.2017.49.4.8>.
- [19] Ramaswamy K, Patham B, Savic V, Tripathy B. Stable and accurate LS-dyna simulations with foam material models: Optimization of finite element model parameters. *SAE Int J Mater Manuf* 2017;10(2):226–33. <http://dx.doi.org/10.4271/2017-01-1338>.
- [20] Fragassa C, Vannucchi de Camargo F, Pavlovic A, Minak G. Explicit numerical modeling assessment of basalt reinforced composites for low-velocity impact. *Composites B* 2019;163:522–35. <http://dx.doi.org/10.1016/j.compositesb.2019.01.013>.
- [21] Vannucchi de Camargo F, Pavlovic A, Schenal EC, Fragassa C. Explicit stacked-shell modelling of aged basalt fiber reinforced composites to low-velocity impact. *Compos Struct* 2021;256:113017. <http://dx.doi.org/10.1016/j.compstruct.2020.113017>.
- [22] Pavlovic A, Fragassa C. Investigating the resistance of reinforced barriers to high velocity projectiles. *Eng Struct* 2018;174:384–95. <http://dx.doi.org/10.1016/j.engstruct.2018.07.074>.
- [23] Jamal-Omidi M, Choopanian Benis A. A numerical study on energy absorption capability of lateral corrugated composite tube under axial crushing. *Int J Crashworthiness* 2019;26(2):147–58. <http://dx.doi.org/10.1080/13588265.2019.1699721>.
- [24] Ghate G, Saify S. Shock tube simulation in LS-Dyna for material failure characterization. *SAE technical paper series*, 2014, <http://dx.doi.org/10.4271/2014-01-0937>.
- [25] Harhash M, Kuhtz M, Richter J, Hornig A, Gude M, Palkowski H. Trigger geometry influencing the failure modes in steel/polymer/steel sandwich crash-boxes: Experimental and numerical evaluation. *Compos Struct* 2021;262:113619. <http://dx.doi.org/10.1016/j.compstruct.2021.113619>.
- [26] Wang J, Zhao J, Liu T, He Z, Li K, Yang W. Crash analysis of composite energy-absorbing cylindrical impact attenuator. *J Reinf Plast Compos* 2015;34(24):2006–17. <http://dx.doi.org/10.1177/0731684415607394>.
- [27] Rogala M, Gajewski J, Gawdzińska K. Crashworthiness analysis of thin-walled aluminum columns filled with aluminum–silicon carbide composite foam. *Compos Struct* 2022;299:116102. <http://dx.doi.org/10.1016/j.compstruct.2022.116102>.
- [28] Fragassa C, Pavlovic A. General considerations on regulations and safety requirements for quadricycles. *Int J Qual Res* 2015;4(9):657–74.
- [29] IIHS. 2023, <https://www.iihs.org/ratings/about-our-tests>.
- [30] EuroNCAP. 2023, <https://www.euroncap.com/en/vehicle-safety/the-ratings-explained/adult-occupant-protection/previous-tests/offset-deformable-barrier/>.
- [31] Martins J, Ribeiro R, Neves P, Brito FP. Accident reconstruction using data retrieval from crash-test video images. *SAE technical paper series*, 2016, <http://dx.doi.org/10.4271/2016-01-1464>.
- [32] Burkhard PM. Closed form solution of BEV's and B1 coefficients from collinear vehicle to vehicle crash testing. *SAE technical paper series*, 2011, <http://dx.doi.org/10.4271/2011-01-0289>.
- [33] Murri R, Caviezel S. Relevance of the IIHS small overlap crash test in Europe. *Manuf Sci Technol* 2014;2(1):1–19. <http://dx.doi.org/10.13189/mst.2014.020101>.
- [34] Hutchinson J, Kaiser MJ, Lankarani HM. The head injury criterion (HIC) functional. *Appl Math Comput* 1998;96(1):1–16. [http://dx.doi.org/10.1016/s0096-3003\(97\)10106-0](http://dx.doi.org/10.1016/s0096-3003(97)10106-0).
- [35] Ruan JS, Khalil TB, King AI. Finite element modeling of Direct Head Impact. *SAE technical paper series*, 1993, <http://dx.doi.org/10.4271/933114>.
- [36] Rondina F, Donati L. Comparison and validation of computational methods for the prediction of the compressive crush energy absorption of CFRP structures. *Compos Struct* 2020;254:112848. <http://dx.doi.org/10.1016/j.compstruct.2020.112848>.
- [37] Ren Y, Zhang H, Xiang J. A novel aircraft energy absorption strut system with corrugated composite plate to improve crashworthiness. *Int J Crashworthiness* 2017;23(1):1–10. <http://dx.doi.org/10.1080/13588265.2017.1301082>.
- [38] Van Ruyven S. Free CAD designs, files and 3D models: The grabcad community library. 2012, URL <https://grabcad.com/library/manikin-test-dummy>.
- [39] Santos K, Silva NM, Dias JP, Amado C. A methodology for crash investigation of motorcycle-cars collisions combining accident reconstruction, finite elements, and experimental tests. *Eng Fail Anal* 2023;152:107505. <http://dx.doi.org/10.1016/j.engfailanal.2023.107505>.
- [40] Dynasupport. 2023, <https://www.dynasupport.com>.
- [41] LS-Dyna, theory manual. 2023.
- [42] André V, Costas M, Langseth M, Morin D. Neural network modelling of mechanical joints for the application in large-scale crash analyses. *Int J Impact Eng* 2023;177:104490. <http://dx.doi.org/10.1016/j.ijimpeng.2023.104490>.
- [43] Toray carbon fabrics. 2020, <https://www.toraycma.com/wp-content/uploads/2511-Prepreg-System.pdf>, journal=2511 prepreg system data sheet - toray composite materials america, Inc..
- [44] Toray honeycomb. 2023, https://www.toraytac.com/media/5527e573-2e72-4aa4-bda7-5a49a20fef06/guunTA/TAC/Documents/Data_sheets/Adhesives_and_Core/Honeycomb_core/Nomex-Honeycomb-Core-Aerospace-Grade_PDS.pdf.
- [45] Sicomin. 2023, <https://sicomin.com/datasheets/product-pdf1139.pdf>, journal=TDS Airex T90 E 1106 - Sicomin.com.
- [46] Federation BP. Polyethylene (high density) HDPE, URL <https://www.bpf.co.uk/plastipedia/polymers/HDPE.aspx>.
- [47] Tsai SW, Wu EM. A general theory of strength for anisotropic materials. 1972, <http://dx.doi.org/10.21236/ada306350>.
- [48] Paolo Feraboli MO. Simulating laminated composite materials using LS-DYNA material model MAT54: Single Element Investigation. *FAA technical report, DOT/FAA/TC-14/19*, 2015.
- [49] Feraboli P, Wade B, Deleo F, Rassaian M, Higgins M, Byar A. LS-Dyna mat54 modeling of the axial crushing of a composite tape sinusoidal specimen. *Composites A* 2011;42(11):1809–25. <http://dx.doi.org/10.1016/j.compositesa.2011.08.004>.
- [50] Berk B, Karakuzu R, Murat Icten B, Arıkan V, Arman Y, Atas C, Goren A. An experimental and numerical investigation on low velocity impact behavior of composite plates. *J Compos Mater* 2016;50(25):3551–9. <http://dx.doi.org/10.1177/0021998315622805>.
- [51] Arachchige B, Ghasemnejad H, Yasaee M. Effect of bird-strike on sandwich composite aircraft wing leading edge. *Adv Eng Softw* 2020;148:102839. <http://dx.doi.org/10.1016/j.advengsoft.2020.102839>.
- [52] Barauskas R, Abraitienė A. Computational analysis of impact of a bullet against the multilayer fabrics in LS-dyna. *Int J Impact Eng* 2007;34(7):1286–305. <http://dx.doi.org/10.1016/j.ijimpeng.2006.06.002>.
- [53] Euroncap. 2020, <https://www.euroncap.com/en/vehicle-safety/glossary/#back>.
- [54] IIHS, frontal offset crashworthiness evaluation guidelines for rating injury measures. 2001, https://www.iihs.org/media/7259ae49-23b6-4f5a-bc66-78c6cc5a5970/sNnnVA/Ratings/Protocols/archive/measures_frontal_0501.pdf.
- [55] Petitjean A, Baudrit P, Trosseille X. Thoracic injury criterion for frontal crash applicable to all restraint systems. *SAE technical paper series*, 2003, <http://dx.doi.org/10.4271/2003-22-0015>.